Condensation on Highly Superheated Surfaces: Unstable Thin Films in a Wickless Heat Pipe

Akshay Kundan*
The Howard P. Isermann Department of Chemical and Biological Engineering, Rensselaer Polytechnic Institute, Troy, New York 12180, USA

Thao T. T. Nguyen†
The Howard P. Isermann Department of Chemical and Biological Engineering, Rensselaer Polytechnic Institute, Troy, New York 12180, USA

Joel L. Plawsky‡
The Howard P. Isermann Department of Chemical and Biological Engineering, Rensselaer Polytechnic Institute, Troy, New York 12180, USA

Peter C. Wayner, Jr.§
The Howard P. Isermann Department of Chemical and Biological Engineering, Rensselaer Polytechnic Institute, Troy, New York 12180, USA

David F. Chao‖
NASA Glenn Research Center Cleveland, Ohio 44135, USA

Ronald J. Sicker¶
NASA Glenn Research Center Cleveland, Ohio 44135, USA

(Received 9 October 2016; revised manuscript received 9 December 2016; published 3 March 2017)

A wickless heat pipe was operated on the International Space Station to provide a better understanding of how the microgravity environment might alter the physical and interfacial forces driving evaporation and condensation. Traditional heat pipes are divided into three zones: evaporation at the heated end, condensation at the cooled end, and intermediate or adiabatic in between. The microgravity experiments reported herein show that the situation may be dramatically more complicated. Beyond a threshold heat input, there was a transition from evaporation at the heated end to large-scale condensation, even as surface temperatures exceeded the boiling point by 160 K. The hotter the surface, the more vapor was condensed onto it. The condensation process at the heated end is initiated by thickness and temperature disturbances in the thin liquid film that wet the solid surface. Those disturbances effectively leave the vapor "superheated" in that region. Condensation is amplified and sustained by the high Marangoni stresses that exist near the heater and that drive liquid to cooler regions of the device.

DOI: 10.1103/PhysRevLett.118.094501

Introduction.—A heat pipe is a device of high thermal conductance used to transport heat over long distances in high heat flux applications. It is an ideal environment for studying how interfacial phenomena affect evaporation and condensation processes. Heat pipe technology has been extensively studied [1–4]. Many articles on micro-heat pipes [2–12], macro-heat pipes [13–15] and V-shaped grooves [16,17] have been published. The phenomena limiting the performance of heat pipes have been discussed theoretically [18–21], demonstrated using temperature and pressure measurements [22–24], and directly visualized in some cases [25]. In any system sustaining large temperature gradients, Marangoni stresses, driven by surface tension differences, arise and may significantly alter flow fields and the processes of evaporation and condensation. Theoretical studies have shown that if enough Marangoni stress is generated in a heat pipe, it should lead to dry out of the hot end and the device will reach its capillary limit earlier [18–20]. Recently, microgravity experiments demonstrated that large Marangoni forces may have the opposite effect and lead to flooding of the heater end, not dry-out [26].

The origins of flooding stem from observations of condensation on subcooled surfaces by Hijikata and Himeno [27] and meniscus evaporation on superheated surfaces by Argade *et al.* [28]. The former found that certain binary vapor mixtures would condense in the form of droplets or streaks even though the two liquids are completely miscible and the vapors of the pure fluids should undergo filmwise condensation. The authors called the phenomenon pseudodropwise condensation. As explained by Hijikata *et al.* [29], the drops were formed by Marangoni flows. Local concentration gradients altered the interfacial tension between liquid and

vapor leading to drop formation. Related phenomena occur in ultrathin films of pure liquids exposed only to temperature gradients leading to film rupture and drop formation [30] or oscillations in a meniscus [31,32].

Here, we demonstrate that condensation of the working fluid on the superheated surface of a wickless heat pipe in microgravity first appears beyond a threshold thermal load to the device and is the source of the flooding phenomenon reported earlier [26]. As we increase the thermal load and raise the temperature at the heated end, the amount of condensed liquid increases. Condensation occurs even as surface temperatures exceed the boiling point by over 160 K. This condensation process arises, is sustained, and is amplified by Marangoni flows.

At this point, we are reporting on a phenomenon for which we have no absolute explanation yet, just snippets of previous models that may help point to an explanation. The purpose of this Letter is to present one curious observation to the community, that as we increase the heat input to the device, we see evidence of increased condensation on the heated surface rather than the expected evaporation and dry-out.

Experimental measurements.—The constrained vapor bubble (CVB) experimental system aboard the International Space Station consisted of a silica cuvette partially filled with pure pentane. A constant heat input was supplied to the heater end, and the cooled end was kept at constant temperature by a cold finger. Thermocouples were installed along one of the walls of the cuvette to measure the temperature profile and interferometry was used to map the liquid film thickness profiles. The experimental details have been described in previous publications [26,33–37] and a synopsis is given in Supplemental Material [38].

Figure 1 shows the temperature profiles in a 40 mm, microgravity CVB experiment carried out using a cold finger temperature of 292 K and electrical power inputs to the heater of 1.6 to 3 W. Beyond 3 W, the heater temperature exceeded the safety limit of 523 K for operation on the space station. The red circles represent the condensation points calculated, using the Antoine equation and experimental pressure measurements [38]. They are a measure of the average vapor temperature. The green markers are the location of the central drop obtained from the vapor-liquid interface images [26] and are the points of maximum evaporation. At positions beyond the green markers, toward the cooled end, the system operates as a classic heat pipe.

Results and discussion.—The liquid distribution within the CVB can be divided into several regions as seen in Fig. 2(a) [35]. The interfacial region is located between the heater end and the "central drop" and first appears at a power input between 0.6 and 0.7 W. At larger power inputs, the temperature gradient was high enough to generate a significant Marangoni flow that drove the liquid away from the heater end. Instead of the heater end becoming dry, liquid accumulated there and reduced the performance of the heat pipe [26,34]. In the sharp corners of the device, the

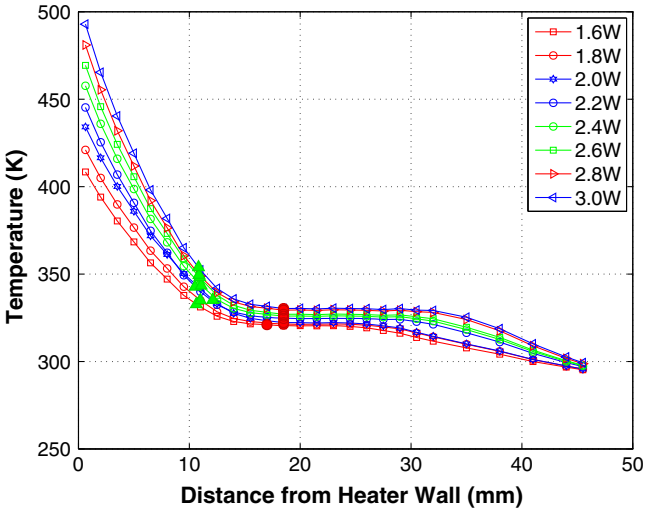

FIG. 1. Temperature profile along the heat pipe.

competition between the capillary return flow and the Marangoni flow formed a junction vortex leading to a thick liquid drop that formed on the flat surface of the cuvette. The balance between the capillary pressure gradient and the Marangoni stress prevented the interfacial region from penetrating further down the heat pipe at power levels in excess of 2.2 W [35]. This can be clearly seen in Fig. S2(b) [38].

In addition to flooding the corners with liquid, the flat surface of the heat pipe in the interfacial region became covered by a wavy film of liquid as highlighted in Fig. 2(b). Though hard to see in Fig. 2(a), as the images at 1.4 and 3.0 W in Fig. 2(b) show, this film became thicker as the heat load was increased. The images suggest that condensation occurred at the heater end, even at temperatures more than 160 K above the normal boiling point (red symbols in Fig. 1).

We used the temperature data from Fig. 1 in conjunction with similar data from an evacuated version of the heat pipe to perform a one-dimensional thermal analysis of the heat flow inside the heat pipe [33]. The results are shown in Figs. 3(a) and 3(b) where the internal heat flow per unit length is plotted versus distance from the heater wall. The negative values in the figures represent net heat loss from the interior wall of the heat pipe while the positive values indicate net heat gain. At power inputs below 0.6–0.7 W where the interfacial region had yet to develop [Fig. 3(b)], we observed only heat loss in the region within 1 cm of the heater wall. We attribute this to evaporation of the liquid there. Once the interfacial region appeared, we observed heat gain near the heater wall whose magnitude grew with the heat input. While we first thought the heat gain was due to increasing radiative exchange with the heater wall, the interference images and growth of the liquid film on the flat portions of the device suggest that the heat gain was due to condensation of vapor in that region. The 5–6 mm nearest the heater wall, where q'_{in} was positive, coincide with the region where we observed the wavy thin film of liquid on the flat surface [Fig. 2(b)]. In addition, the temperature

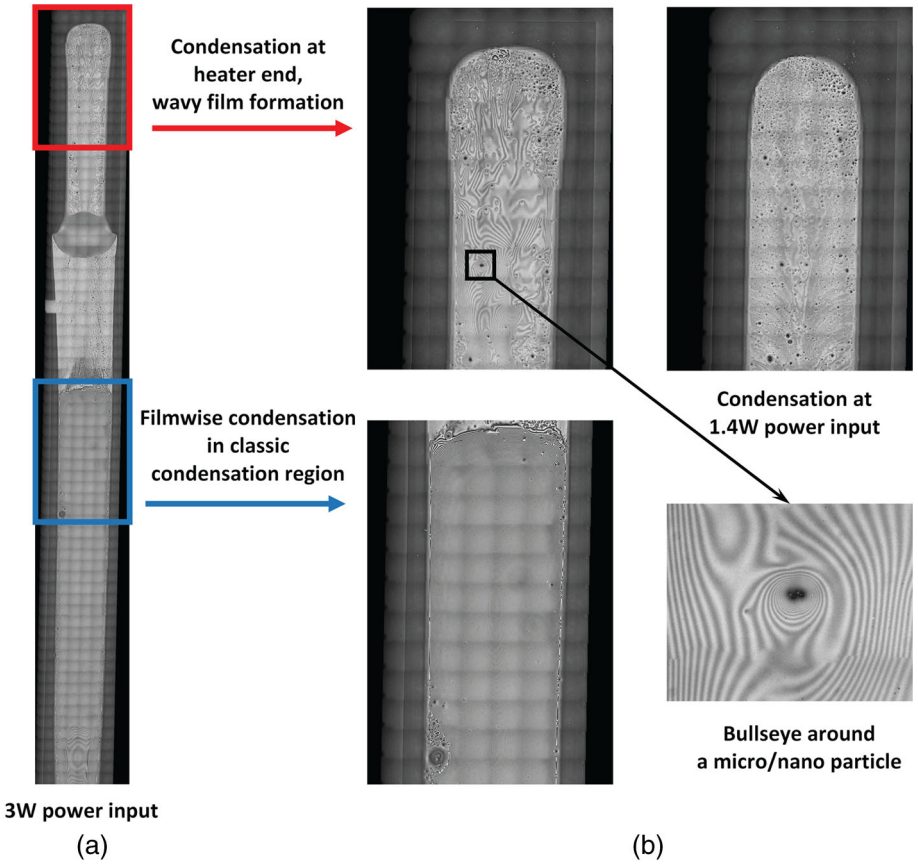

FIG. 2. (a) The interfacial flooding region in the 40 mm microgravity CVB runs [35]. The composite images are comprised of 552 individual microscope frames. (b) Filmwise condensation in the traditional condensation region (lower image) versus the uneven, wavy, film condensation observed near the heater end at 3 and 1.4 W power inputs, respectively (upper images). The density of fringes is larger at 3 W compared to 1.4 W indicating more liquid accumulating on the surface. The bullseye image shows pentane condensing around a microparticle(s).

gradient in this region mimics what is observed in the classic condensation region as shown in Fig. S2(a).

Traditionally, a heat pipe is divided into three consecutive regions: an evaporation zone near the heater, an intermediate or adiabatic zone if the device is insulated, and a condensation zone near the actively cooled region. The images and thermal analysis of the CVB indicate that at least in microgravity, the situation may be more complicated. The normal evaporation zone could be split into a condensation region followed by an evaporation region. There may be an additional, thin evaporation zone on the heater wall upstream of the condensation zone, but we were not able to image that portion of the device.

For a perfectly wetting fluid like pentane on a fused silica surface, only film condensation should occur. Film condensation does occur in the region nearer the cooled portion of the device as shown in the lower image of Fig. 2(b). The film thickness increases monotonically as one approaches the cooled end. By contrast, the region of condensation near the heater end is uneven and at times patchy, suggesting that the physics of the condensation phenomenon involved there is different from that governing the classic condensation region. Temperature gradients along the main axis of the heat pipe can exceed 4000 K/m, while from the center to the edge, they are approximately 750 K/m, enabling strong Marangoni flows from the heater to the cooler end and from the center of the heat pipe toward its edges. The corner flooding in the interfacial region is fed by condensation on the flat surfaces and the flow of that condensate from the center to the edges of the heat pipe.

The remaining question is what drives the condensation at such high surface temperatures? Using the Augmented Young-Laplace equation, the temperature jump at the vapor-liquid interface in the thin film regions of this system was shown to be on the order of 10^{-5} K [35]. Small perturbations to this temperature jump would be sufficient to disturb the "equilibrium" and lead to evaporation or condensation within the film [28,40]. This small perturbation can be created by a change in interfacial curvature that arises from surface roughness variations, liquid composition variations, or micro- or nanoparticles present on the flat surface that were left over from device fabrication. These particles can be seen in Figs. 2(a) and 2(b).

At the very high temperatures near the heater, the unevenness of the wall surface and vapor-liquid interface results in large spatial and temporal perturbations to the film thickness of the kind discussed by Hijikata *et al.* [27,29]. The high temperature gradients near the heater drive the condensed liquid in the interfacial region down the axis of the heat pipe and toward the corners. This prevents the thin film from achieving a steady state, keeps the disjoining pressure higher than the capillary pressure, and amplifies and sustains condensation in that region.

While we see spatial variations in the film thickness, there are also temporal variations that contribute to the condensation. 10× composite images are shown for 1.6, 2.2, 2.8, and 3.0 W in Fig. 4. Each image is composed of

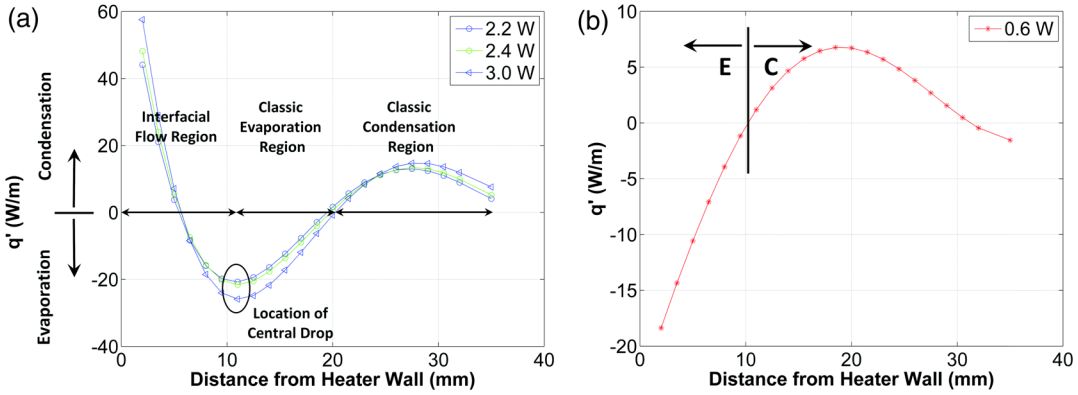

FIG. 3. Heat flow to (positive) or from (negative) the internal surfaces of the heat pipe associated with condensation or evaporation, respectively. (a) High power inputs indicating condensation at the heater end. (b) The heat flow associated with a 0.6 W power input where the interfacial region has not yet developed. The *E* and *C* symbols refer to the traditional heat pipe evaporation and condensation regions.

552 individual frames stitched together, mapping the entire surface of the cuvette. A complete mapping can take 2–3 hours and more details can be found in Supplemental Material [38]. As the whole composite image is comprised of individual images taken at a particular fixed frequency, any abrupt discontinuities within the fringe patterns from frame to frame indicate that the film thickness has changed within the time required to move the microscope stage one frame. Such instabilities are shown and highlighted in Fig. 4. Oscillations in the film thickness are observed all along the main axis of the heat pipe and the frequency, or number, of these oscillations increases with increasing power input. These instabilities lead to more condensation in the interfacial region and ultimately an increase in the adsorbed thin film on the flat surface.

In the context of thin film stability [30–32] for a perfectly wetting fluid, the stabilizing effects are due to the capillary and the disjoining pressures, while vapor recoil, gravity, and the Marangoni stresses tend to destabilize the film. Using models for thin film stability developed and summarized in [41] and a perturbation analysis, we found that the liquid film becomes unstable for wave numbers, k, greater than 0 if

$$\frac{1}{\sigma h_0}\left(\frac{3\alpha_T \Delta\sigma}{2k_T} + \frac{A}{2\pi h_0^3} + \rho g h_0\right) > k^2 > 0. \tag{1}$$

The details of how the equation was derived and the nomenclature used can be found in Supplemental Material [38]. Here, A is the Hamaker constant and $A < 0$ for a perfectly wetting fluid like pentane. Therefore, the thin film is unstable if

$$\underbrace{\frac{3\alpha_T \Delta\sigma}{2k_T}}_{\text{Marangoni stresses}} > \underbrace{\frac{|A|}{2\pi h_0^3}}_{\text{Disjoining pressure}} - \underbrace{\rho g h_0}_{\text{Gravitation}}. \tag{2}$$

The Marangoni term depends on the superheat, $\Delta\sigma = \gamma\,\Delta T_0$. Therefore, at a given film thickness, there is a critical superheat, $\Delta T_{0,C}$, above which the film becomes unstable,

$$\Delta T_{0,C} > \frac{2k_T}{3\alpha_T \gamma}\left(\frac{|A|}{2\pi h_0^3} - \rho g h_0\right). \tag{3}$$

In Fig. 5, we plot the value of $\sigma h_0 k^2$ as a function of liquid film thickness, h_0, for power inputs of 0.7 and 3.0 W. These cases correspond to surface temperatures that were 20 and 160 K above the normal boiling point of pentane at the pressures existing inside the device. 0.7 W represents the power input where instability is first observed, and 3.0 W [34] is the point where the safety limits of the experiment were reached. The gravitational component is always on the order of 10^{-3} Pa or less and so it has a negligible influence on the stability. Gravity does influence the overall performance of the device in 1 g by restricting the return flow of liquid to the heater end. The Marangoni component in Fig. 5 starts to exceed the disjoining pressure component at a film thickness of 67 nm at 0.7 W, and 49 nm

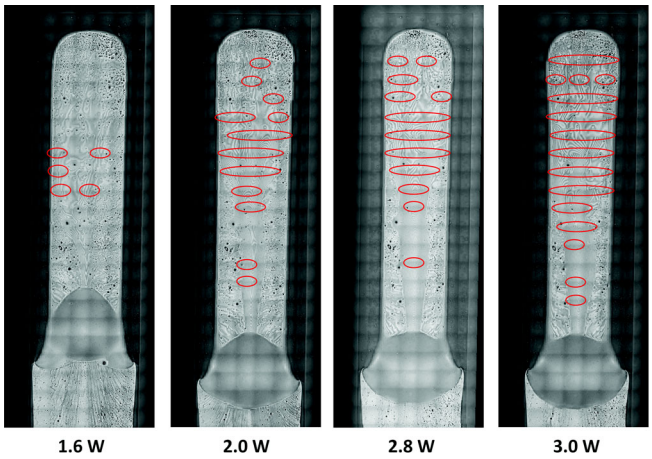

FIG. 4. Interfacial flow region where the ovals highlight regions showing frame-to-frame fringe discontinuities at various power inputs in microgravity. The number of discontinuities increases dramatically with increasing thermal load to the heat pipe.

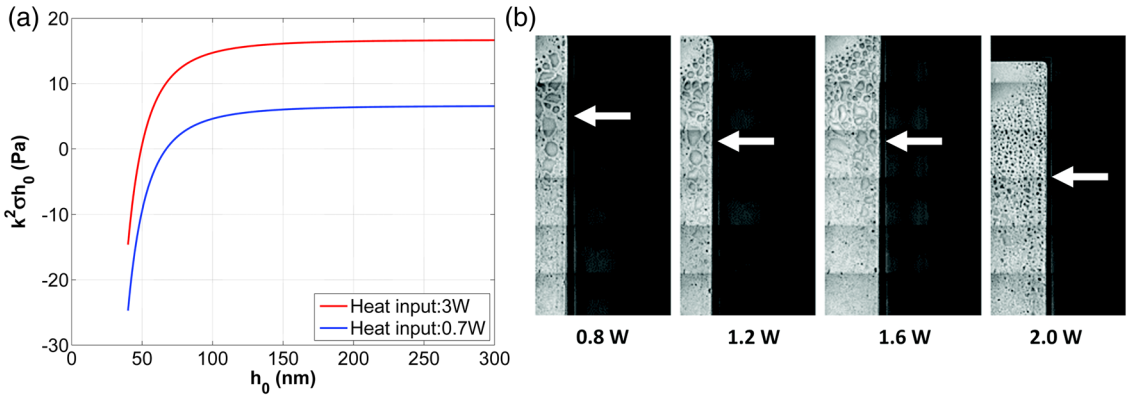

FIG. 5. (a) Scaled wave numbers defining film stability as a function of film thickness. The surface superheat at 0.7 W was 20 K and at 3.0 W was 160 K. Instability occurs when $k^2 > 0$ and this occurs at a thickness above 49 nm at 3 W and 67 nm at 0.7 W. The values for the physical parameters were based on the average temperature at the heater end (heater wall to central drop), and were taken from the NIST database for pentane [42] and [43]. The Hamaker constant was estimated for pentane-on-silica using Lifshitz theory. The value of the heat transfer coefficient α_T was taken from [34] and was calculated based on the models used to generate Fig. 3. (b) 1-g images of the heater end of the CVB showing condensation effects at the heater end. Condensation appears dropwise due to very little return flow in the corners. Full images can be found in Supplemental Material [38].

at 3 W. The first dark interference fringe visible in Fig. 2 occurs at a film thickness of 100 nm when $\lambda = 546$ nm light is used for illumination. Thus, whenever a fringe can be seen on the flat surface of the device near the heater end, the Marangoni component exceeds the disjoining pressure component and the film should be unstable as shown in Fig. 5. At a superheat, $\Delta T_0 \sim 160$ K, and $h_0 \sim 100$ nm, the magnitude of the Marangoni component is approximately 17 Pa and the disjoining pressure is about 2 Pa.

As shown in Figs. 5(b) and S3, the phenomenon also appears in 1 g, if one knows to look for it. However, since the return flow of liquid is meager in 1 g, there is little vapor to condense at the heater end and the phenomenon appears as if pentane were a partially wetting fluid. Thus, it can be easily confused with surface contamination. The droplet density increases and the droplet size decreases with increasing heat input, indicating that it is likely not surface contamination or fluid impurities adsorbing on the surface. The liquid was tested upon returning the device to Earth and was shown to be free of contaminants that might have caused partially wetting behavior.

Conclusions.—Unexpected condensation of liquid on a large scale at the heater end of a wickless heat pipe was observed and analyzed. Small perturbations to the interfacial temperature jump due to the variations in film thickness effectively superheated the vapor and caused the condensation to occur even at temperatures 160 K or more beyond the boiling point. The condensed liquid was driven down the main axis of the heat pipe and from the center of the heat pipe to its edges by strong Marangoni stresses. This led to flooding of the heater end of the device. The thin film within the interfacial/flooded region was spatially and temporally unstable leading to more condensation as the wall temperature was increased. These phenomena also occur in a 1-g environment but are easily mistaken for the effects of surface contamination.

This material is based on the work supported by the National Aeronautics and Space Administration (NASA) under Grant No. NNX13AQ78G and the National Science Foundation under Grant No. CBET-1603318. The raw data and full-resolution composite images are available from NASA's Physical Sciences Informatics System.

A. K. and T. T. T. N. contributed equally to the work.

*akshaykundan@gmail.com
†nguyen.thaoche@gmail.com
‡Corresponding author.
plawsky@rpi.edu
§wayner@rpi.edu
‖David.F.Chao@nasa.gov
¶Ronald.J.Sicker@nasa.gov

[1] T. P. Cotter, in *Proceeding of the 5th International Heat Pipe Conference* (Tsukuba, Japan, 1984), p. 328.
[2] G. P. Peterson, An Introduction to Heat Pipes: Modeling, Testing, and Applications, *Wiley Series in Thermal Management of Microelectronic and Electronic Systems* (Wiley, New York, 1994).
[3] A. Faghri, *Heat Pipe Science and Technology*, 1st ed. (Taylor and Francis, Washington, DC, 1995).
[4] A. Faghri, Review and advances in heat pipe science and technology, J. Heat Transfer **134**, 123001 (2012).
[5] G. P. Peterson, Overview of microheat pipe research and development, Appl. Mech. Rev. **45**, 175 (1992).
[6] D. Khrustalev and A. Faghri, Thermal analysis of a microheat pipe, J. Heat Transfer **116**, 189 (1994).
[7] L. W. Swanson and G. P. Peterson, The interfacial thermodynamics of microheat pipes, J. Heat Transfer **117**, 195 (1995).
[8] B. R. Babin, G. P. Peterson, and D. Wu, Steady-state modeling and testing of a microheat pipe. J. Heat Transfer **112**, 595 (1990).
[9] J. P. Longtin, B. Badran, and F. M. Gerner, A one-dimensional model of a microheat pipe during steady-state operation, J. Heat Transfer **116**, 709 (1994).

[10] H. B. Ma and G. P. Peterson, Experimental investigation of the maximum heat transport in triangular grooves, J. Heat Transfer **118**, 740 (1996).
[11] I. Catton and G. R. Stroes, A semianalytical model to predict the capillary limit of heated inclined triangular capillary grooves, J. Heat Transfer **124**, 162 (2002).
[12] C. P. Migliaccio, K. Dhavaleswarapu, and S. V. Garimella, Temperature measurements near the contact line of an evaporating meniscus *V* groove, Int. J. Heat Mass Transfer **54**, 1520 (2011).
[13] W. J. Bowman, J. K. Storey, and K. I. Svensson, Analytical comparison of constant area, adiabatic tip, standard fins and heat pipe fins, J. Thermophys. Heat Transfer **13**, 269 (1999).
[14] W. J. Bowman, T. W. Moss, D. Maynes, and K. A. Paulson, Efficiency of a constant-area, adiabatic tip, heat pipe fin, J. Thermophys. Heat Transfer **14**, 112 (2000).
[15] W. J. Bowman and D. Maynes, Comparison of standard heat-pipe fins with specified tip temperature condition, J. Thermophys. Heat Transfer **15**, 421 (2001).
[16] B. Suman and N. Hoda, Effect of variations in thermophysical properties and design parameters on the performance of a *V*-shaped microgrooved heat pipe, Int. J. Heat Mass Transfer **48**, 2090 (2005).
[17] X. Xu and V. P. Carey, Film evaporation from a microgrooved surface—an approximate heat transfer model, and its comparison with experimental data, J. Thermophys. Heat Transfer **4**, 512 (1990).
[18] L. Yang and G. M. Homsy, Steady three-dimensional thermocapillary flows and dry-out inside a *V*-shaped wedge, Phys. Fluids **18**, 042107 (2006).
[19] M. Markos, V. S. Ajaev, and G. M. Homsy, Steady flow and evaporation of a volatile liquid in a wedge, Phys. Fluids **18**, 092102 (2006).
[20] R. Savino and D. Paterna, Marangoni effect and heat pipe dry-out, Phys. Fluids **18**, 118103 (2006).
[21] V. S. Ajaev, J. Klentzman, T. Gambaryan, and P. Stephan, Fingering Instability of partially wetting evaporating liquids, J. Eng. Math. **73**, 31 (2012).
[22] R. Savino, N. di Francescantonio, R. Fortezza, and Y. Abe, Heat pipes with binary mixtures and inverse Marangoni effects for microgravity applications, Acta Astronaut. **61**, 16 (2007).
[23] N. di Francescantonio, R. Savino, and Y. Abe, New alcohol solutions for heat pipes: Marangoni effect, and heat transfer enhancement, Int. J. Heat Mass Transfer **51**, 6199 (2008).
[24] K. M. Armijo and V. P. Carey, An experimental study of heat pipe performance using binary mixture fluids that exhibit strong concentration Marangoni effects, J. Therm. Sci. Eng. Appl. **3**, 031003 (2011).
[25] J. M. Ha and G. P. Peterson, Analytical prediction of the axial dry-out point for evaporating liquids in triangular microgrooves, J. Heat Transfer **116**, 498 (1994).
[26] A. Kundan, J. L. Plawsky, P. C. Wayner, Jr., D. F. Chao, R. J. Sicker, B. J. Motil, T. Lorik, L. Chestney, J. Eustace, and J. Zoldak, Thermocapillary Phenomena and Performance Limitations of a Wickless Heat Pipe in Microgravity, Phys. Rev. Lett. **114**, 146105 (2015).
[27] K. Hijikata and N. Himeno, Condensation of azeotropic and nonazeotropic binary vapor mixtures, Annual review of heat transfer **3**, 39 (1990).
[28] R. Argade, S. Ghosh, S. De, and S. DasGupta, Experimental investigation of evaporation and condensation in the contact line region of a thin liquid film experiencing small thermal perturbations, Langmuir **23**, 1234 (2007).
[29] K. Hijikata, Y. Fukasaku, and O. Nakabeppu, Theoretical and experimental studies on the pseudodropwise condensation of a binary vapor mixture, J. Heat Transfer **118**, 140 (1996).
[30] A. Oron, S. H. Davis, and S. G. Bankoff, Long-scale evolution of thin liquid films, Rev. Mod. Phys. **69**, 931 (1997).
[31] A. Chatterjee, Ph.D. thesis, Rensselaer Polytechnic Institute, 2010.
[32] L. Zheng, J. L. Plawsky, P. C. Wayner, Jr., and S. DasGupta, Stability and oscillations in an evaporating corner meniscus, J. Heat Transfer **126**, 169 (2004).
[33] A. Kundan, J. L. Plawsky, and P. C. Wayner, Jr., Thermophysical characteristics of a wickless heat pipe in microgravity—constrained vapor bubble experiment, Int. J. Heat Mass Transfer **78**, 1105 (2014).
[34] A. Kundan, J. L. Plawsky, and P. C. Wayner, Jr., Effect of capillary and Marangoni forces on transport phenomena in microgravity, Langmuir **31**, 5377 (2015).
[35] A. Kundan, T. T. T Nguyen, J. L. Plawsky, P. C. Wayner, Jr., D. F. Chao, and R. J. Sicker, Arresting the phenomenon of heater flooding in a wickless heat pipe in microgravity, Int. J. Multiphase Flow **82**, 65 (2016).
[36] A. Chatterjee, P. C. Wayner, Jr., J. L. Plawsky, D. F. Chao, R. J. Sicker, T. Lorik, L. Chestney, J. Eustace, R. Margie, and J. Zoldak, The constrained vapor bubble fin heat pipe in microgravity, ACS Ind. Eng. Chem. Res. **50**, 8917 (2011).
[37] A. Chatterjee, P. C. Wayner, Jr., J. L. Plawsky, D. F. Chao, R. J. Sicker, T. Lorik, L. Chestney, J. Eustace, R. Margie, and J. Zoldak, Constrained vapor bubble heat pipe experiment aboard the international space station, J. Thermophys. Heat Transfer **27**, 309 (2013).
[38] See Supplemental Material at http://link.aps.org/supplemental/10.1103/PhysRevLett.118.094501 for the experimental apparatus and how the measurements were made, a discussion of how the vapor temperature was calculated, measurements of wall temperature differences between the cuvette center and the corner, a derivation of the model presented in the main paper, and full-scale images of the condensation phenomenon in 1 g, which includes Ref. [39].
[39] J. L. Pawsky, M. Ojha, A. Chatterjee, and P. C. Wayner, Jr., Review of the effects of surface topography, surface chemistry, and fluid physics on evaporation at the contact line, Chem. Eng. Commun. **196**, 658 (2008).
[40] S. J. Gokhale, J. L. Plawsky, and P. C. Wayner, Jr., Experimental investigation of contact angle, curvature, and contact line motion in dropwise condensation and evaporation, J. Colloid Interface Sci. **259**, 354 (2003).
[41] S. H. Davis, in *Perspectives in Fluid Dynamics*, edited by G. K. Batchelor, H. K. Moffatt, and M. G. Worster (Cambridge University Press, Cambridge, 2000), pp. 1–51.
[42] http://webbook.nist.gov/chemistry/fluid/.
[43] *Perry's Chemical Engineers' Handbook*, 7th ed., edited by R. H. Perry, D. W. Green, and J. O. Maloney (McGraw-Hill, New York 1997).